Available online at www.sciencedirect.com
SCIENCE DIRECT®
Journal of the European Ceramic Society 26 (2006) 17–25
www.elsevier.com/locate/jeurceramsoc

Sintering stresses and distortion produced by density differences in bi-layer structures

Dhurjati Ravi*, David J. Green

Department of Materials Science and Engineering, The Pennsylvania State University, University Park, PA 16802, USA

Received 16 July 2004; received in revised form 14 October 2004; accepted 25 October 2004
Available online 5 January 2005

Abstract

The variations in green density that arise when a powder is consolidated gives rise to strain rate incompatibility between regions that can result in densification stresses and or warpage during sintering. In order to quantify the effect of the green density variations, the shrinkage behavior of model bi-layers with a tailored density difference was analyzed. The methodology previously developed for co-firing of layered structures was applied to bi-layers for the case in which the layers do not differ in composition but in density. Alumina tapes with green densities of 1.96 and 2.34 Mg/m^3 were fabricated by tape casting and consolidated into bi-layers. The shrinkage characteristics of the individual layers were characterized and the uniaxial viscosity of the layers with the two starting densities were determined as a function of the degree of densification using cyclic loading dilatometry. The distortion in the bi-layer configurations was experimentally measured and was shown to be in good agreement with the analytical calculations.

Keywords: Sintering; Porosity; Mechanical properties; Al_2O_3; Distortion

1. Introduction

Ceramic materials are commonly fabricated by powder consolidation followed by high temperature heat treatment to achieve the required density. When a powder is consolidated, however, variations in green density are known to arise.[1] These density variations impart a difference in shrinkage strain from one region to another. The corresponding differential strain rate between these regions is expected to produce densification stresses and/or warpage during sintering.[2] From a manufacturing perspective, density gradients could also lead to defect evolution during binder removal process[3] and influence the dimensional tolerance in the final sintered part.[4] The density gradients in single component systems are often a result of the consolidation process. For example, it is known that die wall friction and internal friction between particles lead to gradients in green density for powders compacted under stress.[1]

Although these ideas are well accepted, the need to characterize these density gradients and relate them to the microstructure, properties and tolerances of the final sintered part remains an important research area. One approach is to characterize the density gradients using tools like X-ray tomography, magnetic resonance imaging, ultrasonic velocity[5] or numerical simulations and to use this information in a constitutive model of the densification process. In order to accomplish such a methodology, it is necessary to determine the constitutive properties of a material as a function of green density during the densification process and to use this information to determine the densification stresses and strains. In order to explore this approach, experiments were performed on model bi-layer structures in which there is a green density difference between the layers. If successful, these data can then be used as a starting point for analyzing more complex density distributions using numerical calculations, such as finite element analysis.

* Corresponding author.
E-mail address: dxr235@psu.edu (D. Ravi).

0955-2219/$ – see front matter © 2004 Elsevier Ltd. All rights reserved.
doi:10.1016/j.jeurceramsoc.2004.10.032

Layered ceramic structures are of great technological interest and are commonly employed in electronic packaging applications such as multi-layer ceramic capacitors (MLCC) and solid oxide fuel cells. In recent years, there has been considerable interest in studying the stresses and distortion that occur in the co-firing of these structures. By engineering the structure of individual layers and studying the stress and strain rate behavior of the layers during densification, one can model the stress development and identify the critical parameters to minimize damage or distortion. The current work seeks to apply this methodology to structures in which there is a density difference between the layers rather than a compositional difference.

In order to calculate the stresses in co-fired structures, the elastic and viscous properties of the individual layers have to be determined throughout the densification process. Bordia and Scherer[6,7] suggested that a simple linear viscous constitutive relationship is sufficient to model the mechanical response of a sintering compact during densification. In order to model the sintering behavior, therefore, two viscosity constants, the uniaxial viscosity and the viscous Poisson's ratio, have to be determined as a function of the degree of densification for the selected heating cycle.[6] Various experimental methods have been developed to determine the necessary viscosity constants. One of the earliest techniques used was sinter forging in which a uniaxial constant load was applied on the compact as it sinters: the axial and radial strains were measured continuously with time to resolve the densification and shear rate components.[8,9] Recently, Zuo et al.[10] modified this approach into a discontinuous sinter forging process. As an alternative, Lee et al.[11] determined the uniaxial viscosity by measuring the maximum deflection rate for beams of porous materials that are allowed to deform under their own weight or under applied loads. Another approach proposed by Cai et al.[12] is to use a cyclic load to determine the uniaxial viscosity. In this approach, a cyclic load is applied to the compact as it sinters at a constant heating rate and the change in strain rate due to the application of load is used to calculate the uniaxial viscosity. Gillia et al.[13] have extended this approach to measure the two required viscosity constants. Green et al.[14] have reviewed the scientific and experimental methodology involved in the use of cyclic loading dilatometry in characterizing zirconia-alumina laminates and low temperature co-fired ceramics. In the current work, cyclic loading dilatometry was chosen to characterize the viscous properties of individual layers in the bi-layer structures. This information was then used to predict the distortion behavior of these structures.

2. Experimental procedure

The individual layers in the bi-layer structures were fabricated by casting alumina tapes of different densities. As-received α-alumina powder (A16 SG, Alcoa) with particle size ranging from 0.4 to 0.5 μm was used as the starting powder. In order to produce stable homogeneous slips and achieve good control over the slip rheology, a tape casting procedure involving two-stage dispersion milling was adopted. An azeotropic mixture of methyl ethyl ketone (MEK) (Sigma-Aldrich Corp., St. Louis, MO) and ethyl alcohol was used as the solvent and a polyester/polyamine copolymer (Hypermer KD1, Uniqema Corp, New Castle, DE) was used as the dispersant. The dispersant, MEK, and the ethyl alcohol were added to a polyethylene mill jar that was one-third filled with ZrO_2 media (5 mm in diameter) and milled for 24 h until the dispersant, which is in solid form, was dissolved. Alumina was then added to the mixture and the milling was carried out for another 24 h to break up agglomerates in the powder. The binder and the plasticizer solution consisting of the binder, ethyl methacrylate (Richard E. Mistler Inc, Morrisville, PA) and the plasticizer, butyl benzyl phthalate (Richard E. Mistler Inc, Morrisville, PA) were then added and further milling was carried out for 8 h. The slip was then de-aired in a low-vacuum chamber and cast onto a glass substrate by a batch technique with a doctor blade height of 500 μm and a casting speed of 5 mm/s. The tape was allowed to dry at room temperature for a period of 12 h. In order to obtain tapes of different densities, the solids loading was suitably varied. Two different slip formulations were employed so that tapes of two different green densities could be obtained. The low green density tapes were obtained by decreasing the solids loading in the slip and increasing the organic content. The overall organic content was increased while keeping the ratio of the binder to the plasticizer approximately constant. The slip formulations employed, denoted A and B, and the resultant green densities obtained are given in Table 1. The dried tape was peeled from the glass and punched into 25 mm × 30 mm rectangles. This procedure yielded tapes with a thickness ranging from 120 to 150 μm and with green densities of 1.96 and 2.34 Mg/m^3.

Table 1
Slip formulations and the resultant green densities

Constituent	Function	A (wt.%)	B (wt.%)
Methyl ethyl ketone (MEK)	Solvent	7.21	10.18
Ethyl alcohol	Solvent	7.21	10.18
Polyester/polyamine copolymer	Dispersant	1.07	1.07
Alumina	Ceramic	64.34	54.54
Butyl benzyl pthalate	Plasticizer	4.60	5.44
Ethyl methacrylate: MEK (50:50 wt.%)	Binder	15.57	18.59
Green Density (Mg/m^3)		2.34	1.96

The bi-layer structures were formed by stacking three layers of one density on top of three layers with a different density. Tape-cast ceramic materials often exhibit a great deal of shrinkage anisotropy usually showing greater shrinkage in the *z*-direction when compared to the *x*–*y* casting plane. Although the major shrinkage difference is between the *x*–*y* plane and the *z*-direction, there is some shrinkage anisotropy in the *x*–*y* plane.

The anisotropy in the *x*–*y* plane was controlled to a certain extent during sample preparation by laminating alternate layers using a 90° rotation. That is, one layer was stacked with the tape in the casting direction and followed by a layer

in the transverse casting direction. The typical dimensions for the bi-layers geometry were 75 mm × 3 mm × 1.5 mm. The layered structures were then consolidated by isostatic lamination (Model 1L-4004, Pacific Trinetics Corp., Carlsbad, CA) at 70 °C and 25 MPa for 10 min. The pressed laminates were placed in a low temperature furnace at 450 °C for 6 h for binder burnout. In order to reduce the possibility of defect evolution during binder burnout, slow heating and cooling rates (2 °C/min) were employed. The densities of the samples, after binder burnout, were determined by the Archimedes method using at least six samples for each measurement.

The bi-layer specimens were sintered in a tube furnace for in-situ observation of curling that occurs during sintering. The heating cycle consisted of constant rate heating at 5 °C/min to 1450 °C followed by a hold period of 40 min and eventual cooling at the rate of 10 °C/min. The temperature recordings were made by a thermocouple placed adjacent to the sample. The curvature development was monitored continuously by a video recording device (GR-DVL510U, JVC Corp., Wayne, NJ) as the sample densified. A tinted glass plate (OKI Bering, Cincinnati, OH) was used to control the image contrast. The radius of curvature was measured from the recorded images by drawing an osculating circle through the sample curvature and measuring the radius of the circle drawn. The measurement was made using image processing software (Microsoft Photo Editor).

The shrinkage characteristics of the individual layers were then tested in a thermo-mechanical analyzer (TMA-50, Shimadzu, Columbia, MD). The TMA has a vertical loading rod 3 mm in diameter and measures the shrinkage of the specimen as it sinters. It is also capable of applying controlled loads between 0 and 500 g on the sample through an electromagnetic mechanism. The samples used for the study had dimensions of 3 mm × 3 mm × 4 mm and were made from tapes of constant density. The shrinkage anisotropy in the samples was also investigated by measuring the shrinkage in the z-direction and in the x–y plane in two separate experiments.

The uniaxial viscosity of the individual layers was determined as a function of the degree of densification using the cyclic loading dilatometry technique.[12] The samples were subjected to a 10 min. cyclic loading profile as they sintered under a constant heating rate of 5 °C/min in a dilatometer. Loading and unloading rates of the order of 400 g/min were used. The intended stress was reached within 2 min in each case and it took 2 min for the load to be completely removed. The applied stresses ranged from 0.15 to 0.6 MPa. The change in strain rate due to the load application was used to calculate the viscosity. This can be expressed in mathematical form as

$$\eta = \frac{\sigma_t}{\Delta\dot{\varepsilon}} \tag{1}$$

where σ_t is the applied true stress and $\Delta\dot{\varepsilon}$ is the change in strain rate due to the application of load. The latter was obtained by the difference between the strain rate under load and the free sintering strain rate.

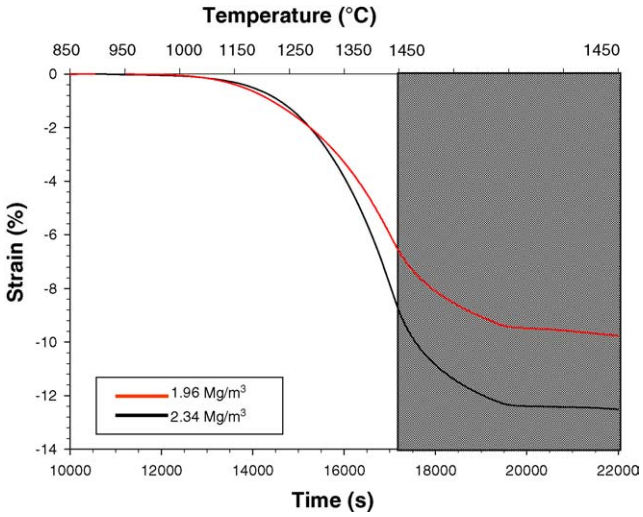

Fig. 1. The shrinkage characteristics of the layers with green densities of 1.96 and 2.34 Mg/m^3 under a constant heating rate of 5 °C/min. The shaded portion of the graph represents a hold period of 40 min at 1450 °C.

The true stress, σ_t, was calculated from the initial stress using the relationship

$$\sigma_t = \frac{\sigma_o}{(1+\varepsilon_f)^2} \tag{2}$$

where σ_o is the initial stress and ε_f is the engineering strain. The final densities of the samples were measured using Archimedes method using at least six samples for each density measurement and the fracture surfaces were examined under the scanning electron microscope (SEM).

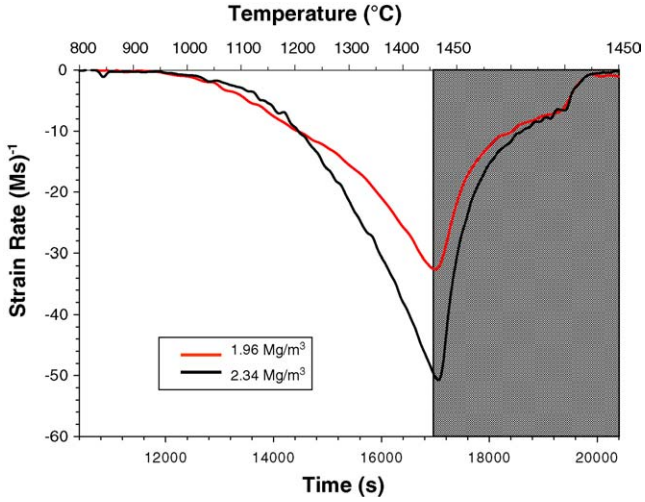

Fig. 2. The strain rate characteristics of the layers with green densities of 1.96 and 2.34 Mg/m^3 under a constant heating rate of 5 °C/min. The shaded portion of the graph represents a hold period of 40 min at 1450 °C.

3. Results and discussion

3.1. Free sintering

The shrinkage characteristics of the high (2.34 Mg/m^3) and low-density layers (1.96 Mg/m^3) are compared in Fig. 1. Although the low-density layer starts to shrink at a slightly lower temperature, the high-density layer soon overtakes it. The contrast in the shrinkage behavior between the high and low-density layers is more clearly shown in Fig. 2, where the shrinkage is plotted in terms of strain rate. During the early stages of sintering, the low-density sample sinters faster than the high-density sample, but at temperatures above 1200 °C the high-density sample has a faster shrinkage rate. At the end of the thermal cycle the high-density sample was found to have a density of 85% of theoretical whereas the low-density sample reaches a density of only about 70% (theoretical density = 3.986 Mg/m^3). A possible reason for the lower densification rate of the low-density material could be the poor particle co-ordination in this layer.

The sintering kinetics and microstructural evolution in a compact are strongly dependent on the starting microstructure and the pore size distribution in the green compact. The excessive amount of organic in the low-density layer presumably decreases the particle coordination and, thus, reduces the shrinkage. The fracture surfaces of the sintered specimen were examined using SEM and are shown in Fig. 3. There was no significant difference in grain size between the high and low-density samples.

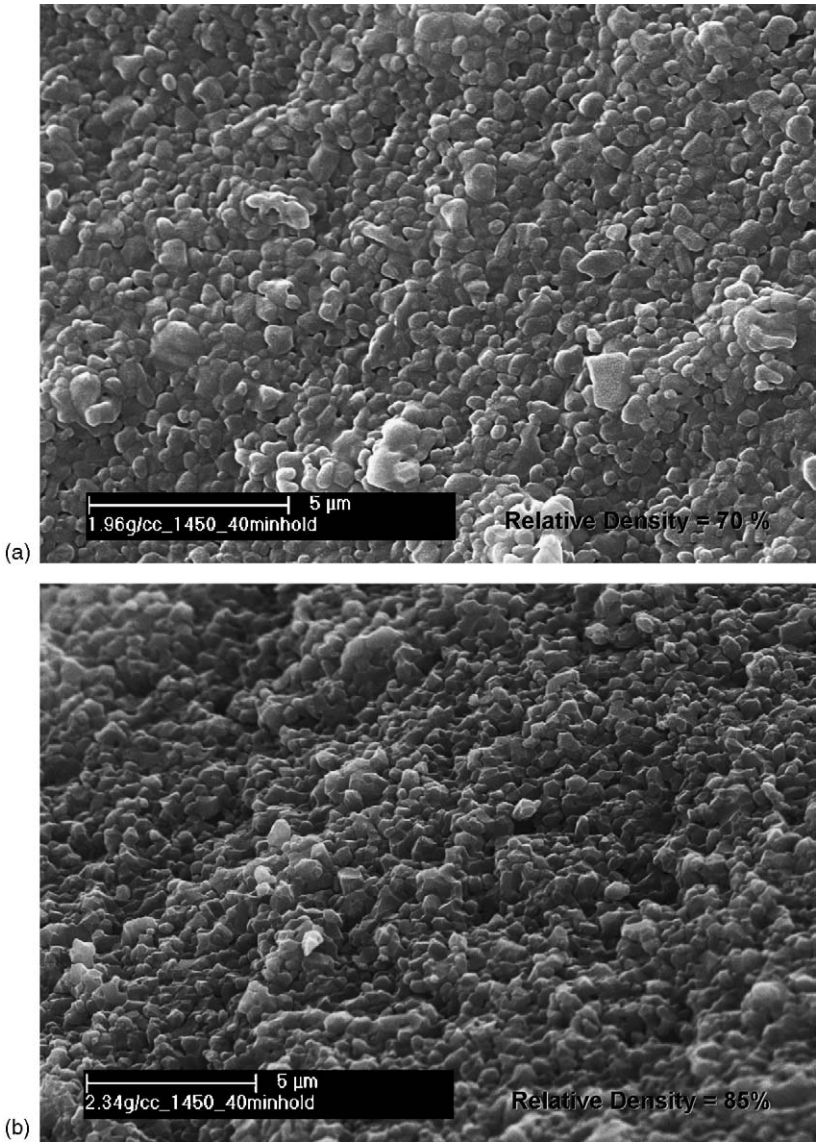

Fig. 3. S.E.M micrographs of fracture surfaces of samples sintered to 1450 °C and held at that temperature for 40 min: (a) green density of 1.96 Mg/m^3 and (b) green density of 2.34 Mg/m^3.

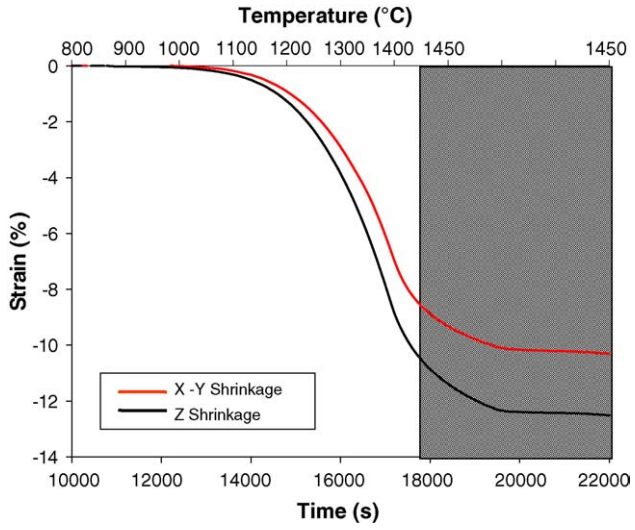

Fig. 4. The shrinkage anisotropy in the layer with green density of 2.34 Mg/m^3.

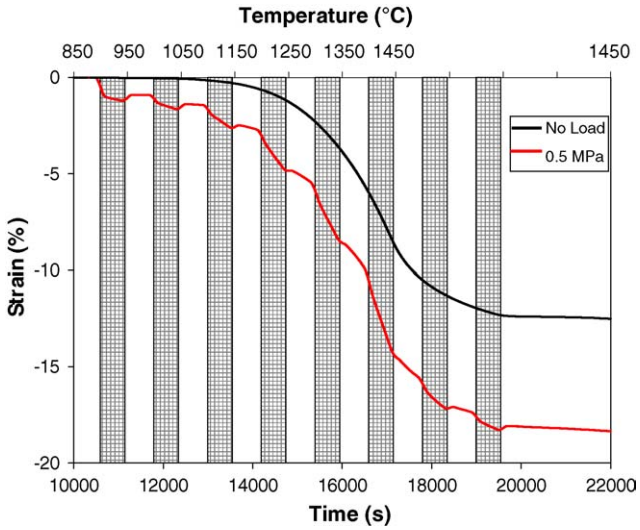

Fig. 5. Linear shrinkage strain under free sintering conditions and under a load of 500 kPa. The shaded portions of the graph represent the period of load application.

3.2. Shrinkage anisotropy

The shrinkage measurements performed using the thermo-mechanical analyzer (TMA) are usually a measure of shrinkage in the z-direction (perpendicular to the casting plane). It is, therefore, important to have an idea of the degree of anisotropy in the samples and take this into account in the density calculations. The degree of anisotropy was investigated by measuring the x–y and z shrinkage in separate experiments and the results are plotted in Fig. 4. The anisotropy factor, k, can be defined as

$$k = \frac{\varepsilon_z}{\varepsilon_{x-y}} \tag{3}$$

where ε_z and ε_{x-y} represent the strain in the z and x–y directions, respectively. Any variation in anisotropy factor was only during the very early stages of sintering (less than 0.5% strain) and for the majority of the sintering process it was found to be constant. The anisotropy factor was found to be 1.3 for the layer with starting density of 2.34 Mg/m^3 and 1.4 for the layer with starting density of 1.96 Mg/m^3. It is important to note that even though the samples exhibit anisotropic shrinkage, the linear viscous model used in the present study assumes the sample behavior to be isotropic.

3.3. Uniaxial viscosity determination

The shrinkage characteristics of the high-density sample with and without the application of a cyclic load are compared in Fig. 5. The thermal cycle consists of constant rate heating at 5 °C/min to 1450 °C, followed by a hold period of 40 min. The shaded regions represent the periods of load application. The final two loading periods occur during the hold period enabling the viscosity to be determined during the hold period. During the initial stages of densification, there is a rapid dimensional change on the application and removal of load indicating an elastic contribution to the overall deformation. However, as the temperature increases, this dimensional change is not easily detected indicating a transition to a viscous regime. At temperatures >1200 °C, the deformation primarily involves change in strain rate during loading. The load-free periods in the load profile are designed to allow the material to relax and once the load is removed, the material recovers its free sintering behavior. This can also be seen in Fig. 6, where the shrinkage characteristics under free sintering and under the application of load are plotted in terms of strain rate. During the load application and removal, there are transient peaks in the strain rate. The strain rate is found to be approximately constant after the load application except in the later stages of the firing cycle. It is quite clear

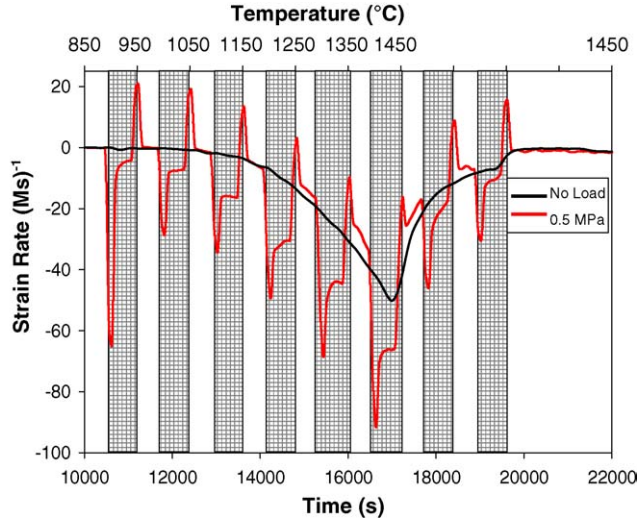

Fig. 6. Linear shrinkage strain rate under free sintering conditions and under a cyclic load of 500 kPa. The shaded portions of the graph represent the period of load application.

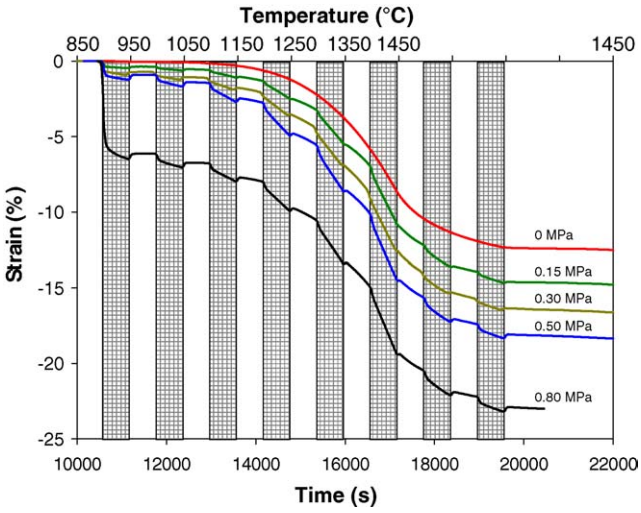

Fig. 7. Linear shrinkage strain under free sintering conditions and under different loads for the layer with green density of 2.34 Mg/m^3.

that the difference in strain rates between the two curves occurs only during the period of load application and once the load is removed, the sample approximately recovers its free sintering behavior.

The uniaxial viscosity of alumina compacts with green densities of 1.96 and 2.34 Mg/m^3 was measured as a function of the degree of densification. The shrinkage curves under different cyclic loads for these compacts are given in Figs. 7 and 8. The stress-induced strain rate was plotted as a function of true stress for various temperatures at which the loading cycle begins, as shown in Figs. 9 and 10. The linear relationship between stress and strain rate is indicated in this plot at the lower temperatures. At the higher temperatures, the data are more scattered and the linearity is less obvious. The uniaxial viscosity was obtained from the slope of the least square fit through the origin for each set of data.

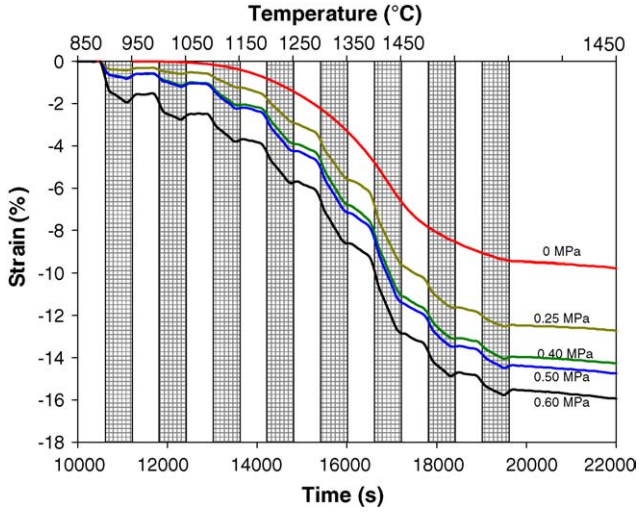

Fig. 8. Linear shrinkage strain under free sintering conditions and under different loads for the layer with green density of 1.96 Mg/m^3.

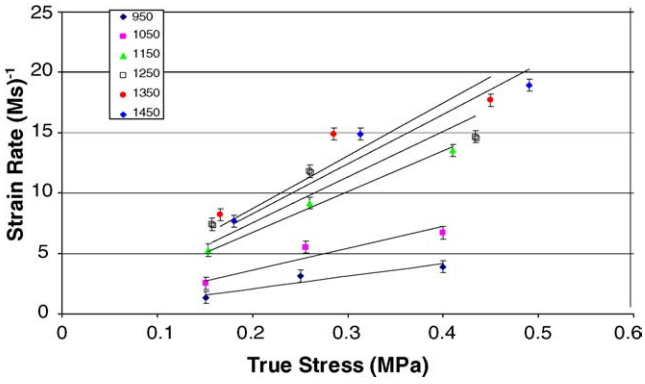

Fig. 9. Stress induced sintering rate as a function of applied uniaxial stress at various temperatures for the layer with green density of 1.96 Mg/m^3.

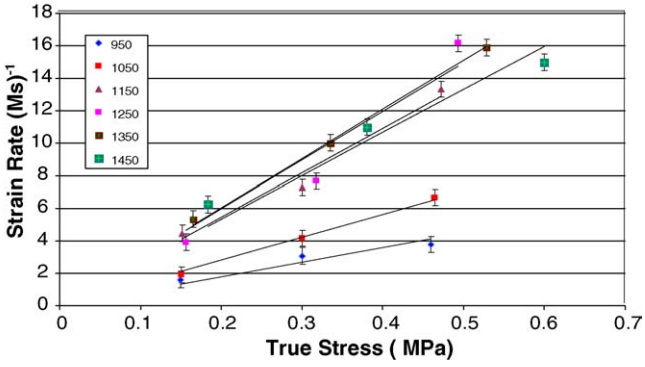

Fig. 10. Stress induced sintering rate as a function of applied uniaxial stress at various temperatures for the layer with green density of 2.34 Mg/m^3.

The uniaxial viscosity thus obtained for the layers with two different starting densities is plotted in Fig. 11 as a function of the relative density. The uniaxial viscosity is primarily dependent on temperature, density and grain size and it is the interplay between these factors that results in the variation of viscosity shown in Fig. 11. During the initial stages of densification, there is a sharp decrease in viscosity with increase in temperature. This is then followed by a period in which

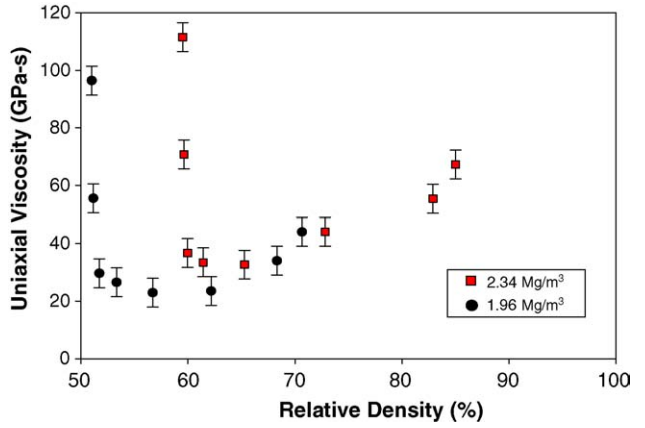

Fig. 11. Measured uniaxial viscosity as a function of relative density for the alumina layers with green densities of 1.96 and 2.34 Mg/m^3.

the viscosity does not undergo a significant change possibly because the decrease in viscosity with temperature is moderated by the increase in viscosity as the material undergoes densification. At the highest densities, the two data sets seem to merge, indicating that the 'memory' of the different initial structure has faded. The uniaxial viscosity data gathered in this study agree well with the earlier experimental measurement of uniaxial viscosity of alumina reported by Cai et al.[12]

3.4. Curvature development in layered structures

The stress development in layered structures during the densification process is dependent on whether the laminate is symmetric or asymmetric. In symmetric structures, stresses arise in the structure but there is no distortion. For asymmetric structures, like the bi-layer, the structure is not only stressed but it also develops a camber. If the bi-layer were to be constrained to be planar, one layer would be primarily in uniform biaxial tension, while the other layer would be in uniform compression. If unconstrained, however, the stresses relax as the structure bends.

If the individual layers in the bi-layer can be considered linear viscous, then the normalized degree of curvature, k, of the bi-layer can be expressed as[15]

$$\dot{k} = \frac{t_1 + t_2}{r} = \frac{6(m+1)^2 mn}{m^4 n^2 + 2mn(2m^2 + 3m + 2) + 1} \Delta\dot{\varepsilon} \qquad (4)$$

where t_1 and t_2, thickness of layers 1 and 2, respectively; r, radius of curvature; m, layer thickness ratio; and n viscosity ratio between layers, $\Delta\dot{\varepsilon}$, strain rate mismatch between the layers. For a plate geometry

$$n = \left(\frac{\eta_1}{1-\upsilon_1}\right)\left(\frac{1-\upsilon_2}{\eta_2}\right) \qquad (5)$$

and for a beam geometry.

$$n = \frac{\eta_1}{\eta_2} \qquad (6)$$

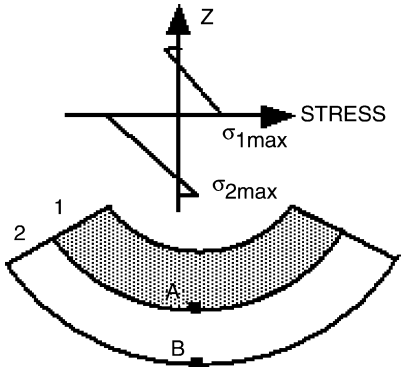

Fig. 12. Curvature development in the bi-layer structure due to strain rate mismatch between the layers. The biaxial stresses vary linearly with thickness and points A and B show the position of the maximum stress in each layer.

The samples used in the present study conform to the beam geometry and, thus, only the uniaxial viscosity is needed to predict the distortion behavior. The viscosity ratio, n, can be obtained using cyclic loading dilatometry, the strain rate mismatch and the thickness ratio can be obtained from the shrinkage data under free sintering conditions and, thus, Eq. (4) can be used to predict the curvature development in a bi-layer from the data gathered in this study.

The stresses in the bi-layer vary linearly with thickness. The largest tensile stress in layer 1 is at the interface (shown by Point A in Fig. 12) and is given by[15]

$$\sigma_1^{\max} = \frac{m^2 n(4m+3)+1}{m^4 n^2 + 2mn(2m^2+3m+2)+1} \eta_1' \Delta\dot{\varepsilon} \qquad (7)$$

A tensile stress may also develop at the outer surface of layer 2 (shown by point B in Fig. 12). The stress at B is given by[15]

$$\sigma_1^{\max} = \frac{m^4 n - m(3m+2)}{m^4 n^2 + 2mn(2m^2+3m+2)+1} \eta_2' \Delta\dot{\varepsilon} \qquad (8)$$

In Fig. 13, the curvature development is recorded in a series of images as the bi-layer sinters under a constant heating rate of 5 °C/min. In this configuration, the layer with higher starting density (2.34 Mg/m^3) is the bottom layer and the one

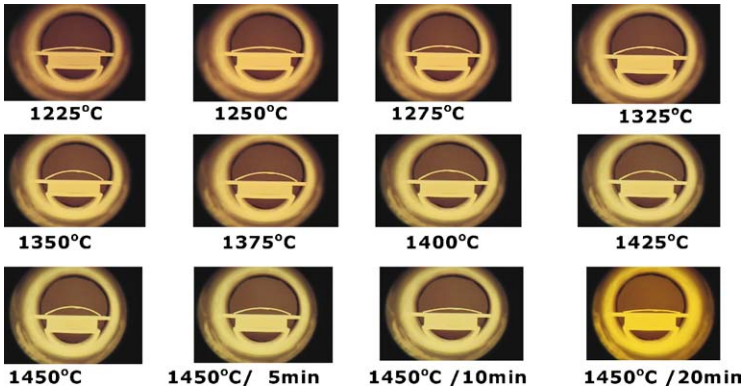

Fig. 13. Series of photographs showing curvature development in the bi-layer geometry with a green density differential of 1.96 vs. 2.34 Mg/m^3 between the layers. The layer with starting density of 1.96 Mg/m^3 is the top layer. The last three images indicate the extent of distortion during the hold period.

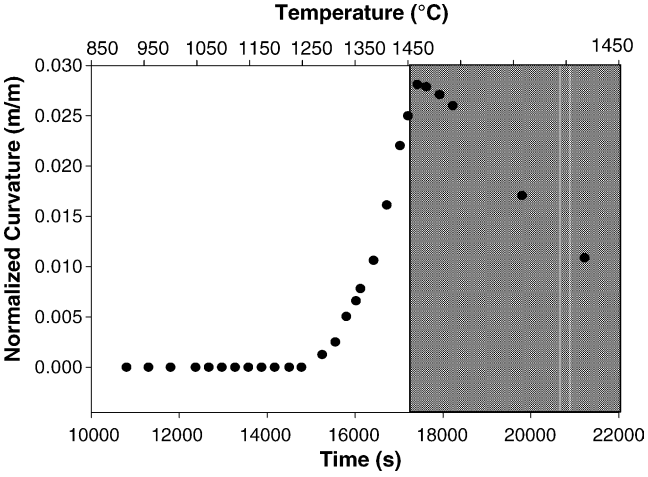

Fig. 14. The distortion in the bi-layer geometry with a green density difference of 1.96 and 2.34 Mg/m^3.

with the lower starting density (1.96 Mg/m^3) forms the top layer. The distortion recorded in the initial stages of densification is due to differential drying during binder burnout. The distortion increases between the temperatures 1250 and 1450 °C. It is a maximum at the start of the hold period and then decreases. The distortion due to differential drying during binder burnout was subtracted from overall distortion, so that the normalized curvature plotted in Fig. 14 is a record of distortion during the densification stage only. The distortion in the bi-layer geometry can be understood in terms of the strain rate mismatch between the individual layers as plotted in Fig. 15, which was obtained from Fig. 2. The layer with the lower starting density sinters faster during the initial stages of densification but for the majority of the sintering process, the layer with the higher green density has faster sintering kinetics. Comparison of Figs. 14 and 15 shows that the distortion closely follows the strain rate mismatch between the layers

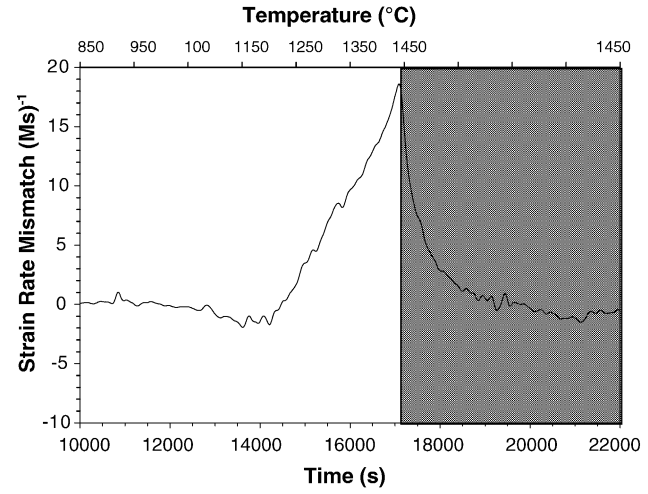

Fig. 15. The strain rate mismatch between the individual layers in the bi-layer geometry with a green density differential of 1.96 and 2.34 Mg/m^3.

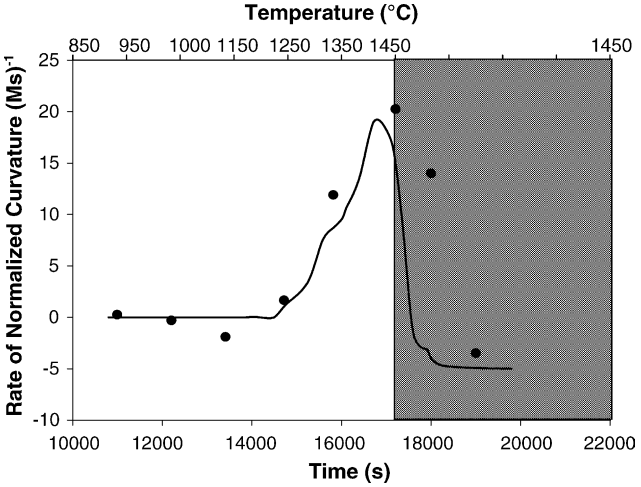

Fig. 16. Comparison between experimentally derived and theoretically calculated rate of normalized curvature for the bi-layer with the green density difference of 1.96 vs. 2.34 Mg/m^3. The solid line represents the experimental values while the data points represent theoretical calculations.

and the maximum distortion occurs at the point of maximum strain rate mismatch (~1450 °C).

The degree of curvature development in a bi-layer depends primarily on the viscosity ratio between the layers, the thickness ratio and the strain rate mismatch between the layers as given by Eq. (4). The experimentally measured curvature values plotted as normalized curvature were differentiated using numerical differentiation method to obtain the rate of normalized curvature. The comparison between the experimentally derived and theoretically calculated values is given in Fig. 16. The analysis indicates a reasonably good agreement between the experimentally derived and theoretically calculated rate of normalized curvature.

The maximum stresses in the bi-layers were also calculated using Eqs. (7) and (8) and the results are shown in Fig. 17. Initially, the stresses are of opposite sign and they

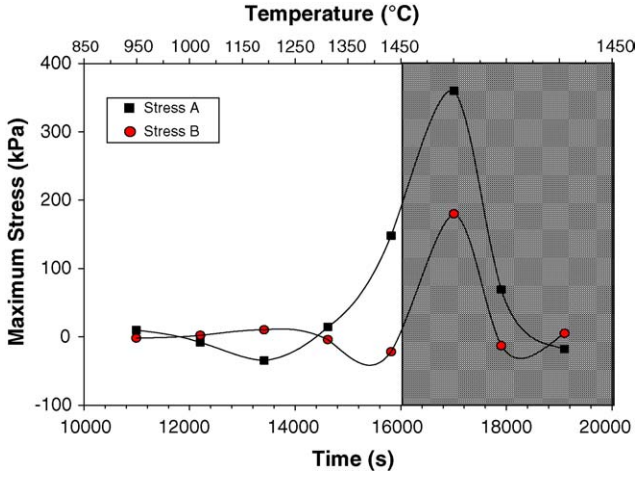

Fig. 17. The calculated maximum stresses that occur in the bi-layer structure during densification.

switch between the layers. The layer in tension is the one that is being subjected to the higher strain rate. In the later stages of sintering as the distortion increases further, the maximum stresses in both layers become tensile. The predicted peak tensile stresses are 180 kPa at point A and 360 kPa at point B and they occur at the point of maximum distortion.

4. Summary and conclusions

The density gradients that develop in ceramic compacts during consolidation are known to cause stresses and damage during the sintering process. In order to quantify the stress development, the methodology that was developed for co-firing of layered structures was applied to structures made of the same material but with a density difference between the layers. Bi-layer structures were fabricated by tape-casting alumina layers of different densities. The green densities obtained were 1.96 and 2.34 Mg/m^3. Dilatometric studies were performed on the strain rate behavior of the individual layers in these structures. The strain rate mismatch between the layers led to distortion in the bi-layers. This distortion was experimentally measured. The uniaxial viscosity of the layers with starting densities of 1.96 and 2.34 Mg/m^3 was calculated as a function of the degree of densification using the technique of cyclic loading dilatometry developed by Cai et al.[12] The uniaxial viscosity and free sintering data were used to calculate the curvature in the bi-layer geometry and these results were compared to those obtained by experiment. The theoretical calculations were found to agree well with experimental results for the bi-layer configurations studied, validating the procedure employed.

Even though the density gradients in ceramic compacts are not uniform but vary in a complex manner (depending on the processing conditions), the use of model layer structures with tailored density gradients was found to be useful in understanding the stress that develops in ceramic compacts due to green density heterogeneity. By characterizing the elastic and viscous properties of these materials as they densify, the incompatibility stresses can be calculated. This understanding could be used as a starting point for calculating stresses in more complex configurations or as an input to numerical calculations.

Acknowledgments

The authors wish to acknowledge the useful advice of Gary Messing and Virendra Puri. The work was supported financially by the NSF-Particulate Materials Center at The Pennsylvania State University.

References

1. Lannutti, J. J., Deis, T. A., Kong, C. M. and Phillips, D. H., Density gradient evolution during dry pressing. *Am. Ceram. Soc. Bull.*, 1997, **76**(1), 53–58.
2. Kellett, B. and Lange, F. F., Stress induced by differential sintering in powder compact. *J. Am. Ceram. Soc.*, 1984, **67**(5), 369–371.
3. Lu, P. K. and Lannutti, J. J., Effect of density gradients on dimensional tolerance during binder removal. *J. Am. Ceram. Soc.*, 2000, **83**(10), 2536–2542.
4. Lu, P. K. and Lannutti, J. J., Density gradients and sintered dimensional tolerance in compacts formed from spray-dried alumina. *J. Am. Ceram. Soc.*, 2000, **83**(6), 1393–1398.
5. Garino, T., Mahoney, M., Readey, M., Ewsuk, K., Gieske, J., Stoker, G. *et al.*, Characterization techniques to validate models of density variations in powder compacts. In *Proceedings of the 27th International SAMPE Technical Conference*, 1995.
6. Bordia, R. K. and Scherer, G. W., On constrained sintering—I. Constitutive model for a sintering body. *Acta Metall.*, 1988, **36**(9), 2393–2397.
7. Bordia, R. K. and Scherer, G. W., On constrained sintering—II. Comparison of constitutive models. *Acta Metall.*, 1988, **36**(9), 2397–2409.
8. Venkatachari, K. R. and Raj, R., Shear deformation and densification of powder compacts. *J. Am. Ceram. Soc.*, 1986, **69**(6), 499–506.
9. Rahaman, M. N., De Jonghe, L. C., Scherer, G. W. and Brook, R. R., Creep and densification during sintering of glass powder compacts. *J. Am. Ceram. Soc.*, 1987, **70**(10), 766–774.
10. Zuo, R., Aulbach, E., Bordia, R. K. and Roedel, J., Critical evaluation of hot forging experiments: case study in alumina. *J. Am. Ceram. Soc.*, 2003, **86**(7), 1099–1105.
11. Lee, S.-H., Messing, G. L. and Green, D. J., Bending creep test to measure the viscosity of porous materials during sintering. *J. Am. Ceram. Soc.*, 2003, **86**(6), 877–882.
12. Cai, P. Z., Messing, G. L. and Green, D. J., Determination of the mechanical response of sintering compacts by cyclic loading dilatometry. *J. Am. Ceram. Soc.*, 1997, **80**(2), 445–452.
13. Gillia, O., Josserond, C. and Bouvard, D., Viscosity of WC–Co compacts during sintering. *Acta Mater.*, 2001, **49**, 1413–1420.
14. Green, D. J., Mohanram, A., Lee, S.-H. and Messing, G. L., Stress development during co-firing of ceramics. In *10th International Conference on Modern Materials and Technologies*, 2002, July 14–18.
15. Cai, P., Green, D. J. and Messing, G. L., Constrained densification of alumina/zirconia hybrid laminates: II Viscoelastic stress computation. *J. Am. Ceram. Soc.*, 1997, **80**(8), 1940–1948.